Dalton Transactions

PAPER

View Article Online
View Journal | View Issue

Cite this: *Dalton Trans.*, 2015, **44**, 5535

On the gold–ligand covalency in linear $[AuX_2]^-$ complexes

Xiao-Gen Xiong,[a,b] Yi-Lei Wang,[b] Cong-Qiao Xu,[b] Yi-Heng Qiu,[b] Lai-Sheng Wang*[c] and Jun Li*[b]

Received 30th December 2014,
Accepted 30th January 2015

DOI: 10.1039/c4dt04031g

www.rsc.org/dalton

Gold compounds, clusters, and nanoparticles are widely used as catalysts and therapeutic medicines; the interactions between gold and its ligands in these systems play important roles in their chemical properties and functionalities. In order to elucidate the nature of the chemical interactions between Au(I) and its ligands, herein we use several theoretical methods to study the chemical bonding in a variety of linear $[AuX_2]^-$ complexes, where X = halogen atoms (F, Cl, Br, I, At and Uus), H, OH, SH, OCH_3, SCH_3, CN and SCN. It is shown that the most important bonding orbitals in these systems have significant contributions from the Au sd hybridized atomic orbitals. The ubiquitous linear or quasi-linear structures of $[AuX_2]^-$ are attributed to the well-balanced optimal overlap in both σ and π bonding orbitals and minimal repulsion between the two negatively charged ligands. The stability of these complexes is related to the covalency of the Au–X bond and a periodic trend is found in the evolution of covalency along the halogen group ligands. The special stability of $[Au(CN)_2]^-$ is a result of strong covalent and ionic interactions. For the superheavy element Uus, the covalency of Au–Uus is enhanced through the spin–orbit interactions.

Introduction

Most of the special properties of gold, including its shiny golden color and its inertness toward air and water, are stemmed from its strong relativistic effects.[1] Over the past few decades, gold complexes and clusters have been extensively studied theoretically and used as model systems to investigate the relativistic effects.[2] Compared with its lighter congeners, copper and silver, gold has an unusually large electron affinity (EA) and ionization potential (IP) due to the relativistic contraction and stabilization of the 6s orbital.[3] Hence, the Au 6s orbital is more electrophilic than the 4s orbital in Cu and the 5s orbital in Ag.[2g] At the same time, indirect relativistic effects destabilize the Au 5d orbitals.[1b] Consequently, the 5d–6s energy gap is significantly reduced, resulting in the optical absorption of bulk gold (and hence its golden color) and making sd hybridization favorable in the Au atom.[4] One of the direct consequence of the sd hybridization is the various known oxidation states of Au, ranging from −1 to +5.[5] In recent decades, there has been a renaissance in gold chemistry, in particular, due to the discovery of interesting catalytic effects in gold nanoparticles and organogold complexes.[6] Gold-containing compounds have been used as therapeutic medicines even in the ancient times.[7] Gold has been known to form coordination compounds with organic groups, halides, thiolates, phosphanes, and most extraordinarily with the noble gases, as found in recent experimental and theoretical studies.[8] In addition to the increased experimental activities in gold chemistry, there has also been a remarkable growth in the theoretical chemistry of gold, as extensively reviewed in a series of articles by Pyykkö.[9]

One of the most common oxidation states of gold is Au(I) with a coordination number of two and usually in a linear geometry.[10] The preference of coordination number two in Au(I) has been shown to be strengthened by relativistic effects.[2c] Gold 5d contributions to the Au–X bond have been enhanced through relativistic expansion of the 5d orbitals. Au(I)-complexes are a class of highly efficient and selective homogeneous catalysts for a number of important organic transformations.[6c,11] R_3PAuX (X = other coordinating counterions) species are formed in the seminal work of cationic phosphine–Au(I) species in catalyzing the hydrogenation of alkynes. As already mentioned by Toste[6c], besides the well-studied Au(I)–phosphine species, other ligands can be used to tune the "acidity" of Au(I) in order to influence the catalyst reactivity. Au(I)-complexes involve extensive aurophilic interactions and can be used as building blocks in supramolecular design.[12] In recent years,[13] we have used state-of-the-art photoelectron

[a]*Shanghai Institute of Applied Physics, Chinese Academy of Sciences, Shanghai 201800, China*
[b]*Department of Chemistry & Key Laboratory of Organic Optoelectronics and Molecular Engineering of Ministry of Education, Tsinghua University, Beijing 100084, China. E-mail: junli@mail.tsinghua.edu.cn*
[c]*Department of Chemistry, Brown University, Providence, RI 02912, USA. E-mail: lai-sheng_wang@brown.edu*

spectroscopy and sophisticated theoretical methods to study a series of Au(I) compounds in the gas phase, including $[AuH_2]^-$, $[AuI_2]^-$, $[Au(CN)_2]^-$, $[XAuCN]^-$ (X = halogens), and most recently Au(I)-acetylides.[14] With the help of theoretical calculations and bonding analyses, photoelectron spectra of these negatively charged Au(I) complexes, many of which are observed for the first time in the gas phase, have been quantitatively interpreted, allowing the chemical bonding between Au(I) and the ligands to be elucidated. A common feature among these compounds is that Au(I) forms distinct, albeit weak, covalent bonding with different ligands.[15] However, it is expected that the degree of covalency should depend on the ligand. It would be interesting to systematically investigate the nature of the Au(I) bonding with different ligands to discover general principles and periodic trends. In this article, we present such a systematic theoretical study of the Au(I)–X bond with a variety of ligands in $[AuX_2]^-$ for X = halogens (including At and Uus), H, OH, SH, OCH_3, SCH_3, SCN and CN. The insight and trend obtained in the current work on the Au(I)–ligand bonding and its dependence on the different types of ligands should be valuable to understand the chemistry of gold complexes and help design more effective and specific homogeneous gold catalysts.

Theoretical methods

Chemical bond analyses

Pure ionic bonding is only an ideal model. In reality, all ionic bonds have some characters of electron sharing between the two bonded atoms, that is, a balance always exists between ionic and covalent bonding. Therefore, an exact wave function for a molecular system can always be partitioned into ionic and covalent components. Many theoretical methods have been used to measure the covalency of a chemical bond. Electron localization functions (ELFs)[16] and natural resonance theory (NRT)[17] are chosen in this article to both qualitatively and quantitatively measure the covalency of gold–ligand bonds. ELF is a chemically intuitive approach to show the difference between ionic and covalent bonds. Usually a large ELF value between two atoms reflects a high electron-pair density between them or, in other words, high apparent covalent bonding. NRT is a method based on the first-order reduced density matrix and its representation in terms of natural bond orbitals (NBOs). The NRT approach allows the expansion of total wave function in terms of chemically intuitive resonance structures.[17a] Since NRT results are subject to the choice of reference resonance structures, the same reference resonance structures should be chosen consistently in order to make meaningful comparisons among congeners. In the current work, the resonance structures of X^- Au–X ↔ X–Au X^- are used for all the molecules.

Energy decomposition analyses

Bonding energy is an important criterion for the stability of a chemical bond. Energy decomposition analysis (EDA)[18] is used in this article to access different contributions to bonding energies. According to EDA, the interaction energy between two atoms or two fragments can be decomposed into the sum of electrostatic interactions, Pauli repulsion, and the orbital interaction energy:

$$\begin{aligned}\Delta E_{\text{bonding}} &= \Delta E_{\text{electrostatic}} + \Delta E_{\text{pauli}} + \Delta E_{\text{orbint}} \\ &= \Delta E_{\text{steric}} + \Delta E_{\text{orbint}}\end{aligned} \quad (1)$$

The sum of the electrostatic interaction energy and Pauli repulsion is also called the steric interaction energy. The orbital interaction can be viewed as an electron transfer from one fragment to the other or it can be pictured as the orbital mixing between two fragments. An ionic bond can be described as the interaction between two frozen densities plus intramolecular relaxations, which is ΔE_{steric} in the language of EDA. So the orbital interaction energy in the total bonding energy reflects the degree of covalency in the chemical bond between two atoms or fragments.

Computational methods

The geometries of the molecules are optimized at the generalized gradient approximation (GGA) level with the PBE exchange–correlation functional,[19] as implemented in the Amsterdam Density Functional (ADF 2009.01) program.[20] The scalar-relativistic (SR) effects are taken into account by the zero-order-regular approximation (ZORA).[21] For heavy elements, spin–orbit (SO) splitting[22] is also considered by the ZORA method with the SR-ZORA optimized geometries. The geometries are confirmed to be minima through the vibrational frequency calculations at the same level. For the geometry optimization and vibrational frequency calculations, the Slater basis sets with the quality of triple-ζ plus two polarization functions (TZ2P) are used with the frozen core approximation applied to the inner shells $[1s^2–4f^{14}]$ for Au, $[1s^2]$ for C, N, O and F, $[1s^2–2p^6]$ for Cl and S, $[1s^2–3d^{10}]$ for Br, $[1s^2–4d^{10}]$ for I, $[1s^2–5d^{10}]$ for At, and $[1s^2–5f^{14}]$ for Uus. In order to further investigate the variation of the Au–X bond length along with the electron correlation methods, the geometries of the ground state are also optimized with MP2,[23] SCS-MP2,[24] CCSD[25] and CCSD(T)[26] methods, as implemented in Molpro 2008.[27] The Stuttgart energy-consistent relativistic pseudopotentials ECP60MDF (Au), ECP60MDF (At) and ECP28MDF (I) and the corresponding augmented valence triple-ζ basis sets aug-cc-pVTZ-PP are used for Au,[28] At,[29] and I.[30] The all-electron basis sets aug-cc-pVTZ is used for the other atoms.[31] For convenience, we will call the basis sets used in the Molpro calculations as AVTZ hereafter.

The NBO and NRT calculations are performed using the NBO 5.0 package,[32] with the wave function of each molecule generated at the level of PBE exchange–correlation functional, as implemented in Gaussian 09.[33] The pseudopotentials and basis sets used in Gaussian 09 calculations are the same with the above-mentioned Molpro calculations, we will also call the

basis sets used in the Gaussian 09 calculations as AVTZ from now on. For X = H, F–At, CN, OH, and SH, we also carried out NBO and NRT calculations with the wave function generated at the level of CCSD, while the calculations of the density matrix were done through the orbital-optimized coupled-cluster doubles method (OOCCD).[34] OOCCD calculations were performed with Orca,[35] and the segmented all-electron relativistically-contracted (SARC) basis sets[36] were used for all atoms. In order to handle the relativistic effects, we used second order Douglas–Kroll–Hess approximation (DKH2) in the Orca calculations.

To compare the bond strengths *via* vibrational frequencies, we have also calculated the so-called normalized vibrational frequencies (NVF) for $[AuX_2]^-$ at the PBE level, which eliminates the difference of the reduced mass of this series of molecules.[12c] The EDA between AuX and X^- is also based on the PBE/TZ2P calculations with the SR-ZORA Hamiltonian. The ELF calculations are performed with the DENSF utility of the ADF program, for which the all-electron Slater basis sets with the quality of triple-ζ plus two polarization functions (TZ2P) are used.

Results and discussion

Geometry optimizations show that the $[AuX_2]^-$ complex indeed prefers linear $[X–Au–X]^-$ structures for X = H, halogen atoms, CH_3, OCH_3, and CN, whereas it is slightly bent for X = OH, SH, SCH_3, and SCN. The optimized geometries of the ground state at the level of PBE and various electron correlation methods are given in Tables 1 and 2. The results of NBO and NRT analyses at the level of PBE/AVTZ are presented in Table 3. The EDA analyses between AuX and X^-, on the basis of ADF calculations, are presented in Table 5. The ELF results (Fig. 1 and 4) are all based on the PBE optimized geometries.

Table 1 The geometry and structural parameters of $[AuX_2]^-$ at the level of SR-ZORA PBE/TZ2P. All lengths are in Å and all angles are in degree

X	Symm.	R(Au–X)	∠(X–Au–X)	X	Symm.	R(Au–X)	∠(X–Au–X)
H	$D_{\infty h}$	1.670	180.00	CN	$D_{\infty h}$	1.995	180.00
F	$D_{\infty h}$	1.996	180.00	CH_3	D_3	2.110	180.00
Cl	$D_{\infty h}$	2.305	180.00	OH	C_2	2.032	177.26
Br	$D_{\infty h}$	2.454	180.00	SH	C_2	2.331	179.00
I	$D_{\infty h}$	2.611	180.00	OCH_3	C_{2h}	2.030	180.00
At	$D_{\infty h}$	2.715	180.00	SCH_3	C_2	2.321	177.80
Uus	$D_{\infty h}$	2.814	180.00	SCN	C_2	2.318	174.77

Table 2 The optimized bond length of Au–X in $[AuX_2]^-$ at the level of MP2, SCS-MP2, CCSD and CCSD(T). The PBE calculated bond lengths are also listed for comparison. All bond lengths are in Å

	PBE(ADF)	MP2	SCS-MP2	CCSD	CCSD(T)
H	1.670	1.622	1.633	1.649	1.647
F	1.996	1.945	1.955	1.961	1.963
Cl	2.305	2.237	2.261	2.284	2.280
Br	2.454	2.348	2.374	2.400	2.394
I	2.611	2.512	2.540	2.567	2.561
At	2.715	2.586	2.616	2.644	2.639
Uus	2.814	2.670	2.703	2.736	2.731
CN	1.995	1.953	1.973	1.993	1.988
OH	2.032	1.975	1.988	1.995	1.998
SH	2.331	2.258	2.282	2.306	2.301

$[AuX_2]^-$: X = F–Uns

To access the trend down the periodic table, we have performed systematic studies of $[AuX_2]^-$ for all the halogens from F to Uus. Table 1 shows the Au–X bond length increases from F to Uus for the halogen series. For X = F–I, our PBE Au–X bond lengths are around 0.03–0.05 Å shorter than previous reports of configuration interaction calculations with singles and doubles corrected by size-consistency effects.[2c] However, our PBE Au–X bond lengths are slightly longer for X = Cl, Br, and I, compared to CCSD(T) (coupled-cluster with singles and doubles and perturbative triple excitations) benchmark calculations by Mishra,[37] who used augmented correlation-consistent polarized valence quadruple-ζ (aug-cc-pVQZ) basis sets. Single point CCSD(T) calculations based on the MP2-optimized geometry for $[AuF_2]^-$ was also performed by Schwerdtfeger and co-workers, who suggested the stability of $[AuF_2]^-$ is enhanced through relativistic effects.[38] As an example of how the electron correlation affects the theoretical geometries of $[AuX_2]^-$, the bond lengths with different electron correlation methods are also given in Table 2. Our CCSD(T)/AVTZ calculations show that the Au–X bond length for X = Cl, Br, and I are 0.004–0.015 Å shorter than Mishra's results; and the bond lengths calculated for X = F–I using MP2/AVTZ are 0.09–0.14 Å shorter than Schwerdtfeger's results based on MP2 calculations.[2d] The relatively large deviation of the MP2 bond lengths in the present study compared with those by Schwerdtfeger are due to differences of the basis sets used. In Schwerdtfeger's later work, the bond length of Au–F in $[AuF_2]^-$ was reported to be 1.959 Å, which is closer to the present results than the previous reports.[38] Compared with CCSD(T) calculations, MP2 underestimates the Au–X bond length for all halogen atoms, while SCS-MP2 gives relatively improved results over MP2. CCSD overestimates the bond length for X = Cl–Uus, but underestimates it for X = F.

The NBO and NRT results listed in Table 3 show increasing covalency of the Au–X bond down the periodic table for the X = halogens. The covalent contribution in the Au–F bond is relatively small and the Au–F bond can be treated as mainly ionic, while the covalent contribution in Au–I reaches to about 44%. NBO analyses of the Au–X bond reveal that the bonding orbitals all have significant contributions from the Au sd hybridized atomic orbitals (AOs) and the composition of ligand AOs decreases from F to Uus. The trend of the ELFs in the bond region is consistent with the NRT results for the Au–halogen bonding, as shown in Fig. 1. The theoretical atomic charges calculated using different charge-density partition schemes are given in Table 6. As expected, all the halogen atoms are negatively charged with the absolute values of the negative charge decreasing from F to Uus, consistent with the increased electronegativity of the halogens. Our further NBO and NRT results based on CCSD-DKH2/SARC calculations show the

Table 3 Natural bond orbital (NBO) analyses and natural resonance theory (NRT) bond order (BO) of the Au–X bond in $[AuX_2]^-$ at the PBE/AVTZ level[a]

		NRT BO		
X	NBO analysis	Covalent	Ionic	Covalent/total[b]
H	35.92% $(sp^{0.01}d^{0.19})_{Au}$ + 64.08% $(s)_H$	0.275	0.177	0.609
F	14.85% $(sp^{0.01}d^{0.43})_{Au}$ + 85.15% $(sp^{7.26}d^{0.01})_F$	0.138	0.362	0.276
Cl	20.67% $(sp^{0.01}d^{0.21})_{Au}$ + 79.33% $(sp^{6.98}d^{0.02})_{Cl}$	0.184	0.316	0.368
Br	22.69% $(sp^{0.01}d^{0.17})_{Au}$ + 77.31% $(sp^{8.41}d^{0.02})_{Br}$	0.200	0.301	0.398
I	25.76% $(sp^{0.01}d^{0.12})_{Au}$ + 74.24% $(sp^{9.79}d^{0.02})_I$	0.221	0.279	0.441
At	27.09% $(sp^{0.01}d^{0.11})_{Au}$ + 72.91% $(sp^{14.78}d^{0.02})_{At}$	0.229	0.271	0.459
Uus	29.21% $(sp^{0.01}d^{0.11})_{Au}$ + 70.79% $(sp^{27.47}d^{0.02})_{Uus}$	0.243	0.257	0.486
CH_3	27.73% $(sd^{0.30})_{Au}$ + 72.27% $(sp^{3.15})_C$	0.233	0.275	0.459
OH	18.69% $(sp^{0.01}d^{0.44})_{Au}$ + 81.31% $(sp^{6.22}d^{0.02})_O$	0.169	0.331	0.338
SH	25.66% $(sp^{0.01}d^{0.19})_{Au}$ + 74.34% $(sp^{6.38}d^{0.03})_S$	0.220	0.284	0.436
OCH_3	19.26% $(sd^{0.46})_{Au}$ + 80.74% $(sp^{7.78}d^{0.02})_O$	0.168	0.318	0.346
SCH_3	27.90% $(sd^{0.21})_{Au}$ + 72.10% $(sp^{7.10}d^{0.04})_S$	0.231	0.262	0.468
CN	26.84% $(sd^{0.27})_{Au}$ + 73.16% $(sp^{1.07})_C$	0.224	0.307	0.423
SCN	26.26% $(sp^{0.01}d^{0.18})_{Au}$ + 73.74% $(sp^{10.04}d^{0.05})_S$	0.211	0.261	0.447

[a] VQZ-PP basis set was used for Uus.[14] [b] Total means the sum of the covalent and ionic bond order.

Table 4 Natural bond orbital (NBO) analyses and natural resonance theory (NRT) bond order (BO) of the Au–X bond in $[AuX_2]^-$ at the CCSD-DKH2/SARC level

		NRT BO		
X	NBO analysis	Covalent	Ionic	Covalent/total[a]
H	32.11% $(sp^{0.01}d^{0.20})_{Au}$ + 67.89% $(s)_H$	0.252	0.207	0.549
F	12.54% $(sp^{0.01}d^{0.46})_{Au}$ + 87.46% $(sp^{6.19}d^{0.01})_F$	0.116	0.374	0.237
Cl	18.10% $(sp^{0.01}d^{0.22})_{Au}$ + 81.90% $(sp^{6.36}d^{0.03})_{Cl}$	0.160	0.324	0.331
Br	19.21% $(sp^{0.02}d^{0.18})_{Au}$ + 77.31% $(sp^{7.27}d^{0.03})_{Br}$	0.168	0.315	0.348
I	22.60% $(sp^{0.02}d^{0.13})_{Au}$ + 77.40% $(sp^{7.00}d^{0.01})_I$	0.193	0.286	0.402
At	22.07% $(sp^{0.02}d^{0.11})_{Au}$ + 77.93% $(sp^{10.34}d^{0.03})_{At}$	0.189	0.290	0.394
OH	16.30% $(sp^{0.01}d^{0.46})_{Au}$ + 83.70% $(sp^{5.28}d^{0.01})_O$	0.131	0.271	0.326
SH	22.93% $(sp^{0.01}d^{0.20})_{Au}$ + 77.07% $(sp^{5.74}d^{0.04})_S$	0.272	0.332	0.450
CN	23.58% $(sd^{0.26})_{Au}$ + 76.42% $(sp^{0.83})_C$	0.184	0.259	0.416

[a] Total means the sum of the covalent and ionic bond order.

Table 5 Energy decomposition analyses for $[XAuX]^- \rightarrow AuX + X^-$. The last column is the ratio of the orbital interaction and total interaction energy. The results are based on the SR-ZORA PBE/TZ2P calculations. All energies are in eV

	Steric					
X	Electrostatic	Pauli	Sum	Orbital interaction	Total	Orb./total
H	−10.12	9.09	−1.06	−2.77	−3.84	0.72
F	−5.48	3.90	−1.58	−2.69	−4.26	0.63
Cl	−5.51	4.62	−0.89	−2.52	−3.41	0.74
Br	−5.12	4.33	−0.79	−2.32	−3.11	0.75
I	−5.04	4.51	−0.53	−2.36	−2.88	0.82
At	−4.65	4.24	−0.41	−2.28	−2.69	0.85
Uus	−4.54	4.36	−0.18	−2.33	−2.52	0.93
OH	−6.41	5.12	−1.29	−2.99	−4.28	0.70
SH	−7.16	6.55	−0.61	−2.82	−3.42	0.82
OCH_3	−5.59	4.90	−0.69	−3.05	−3.74	0.82
SCH_3	−7.41	7.02	−0.39	−3.00	−3.39	0.88
CN	−9.32	7.84	−1.49	−3.16	−4.65	0.68
SCN	−5.87	5.56	−0.30	−2.85	−3.15	0.90
CH_3	−9.48	8.33	−1.16	−2.83	−3.99	0.71

Table 6 Theoretical atomic charges on Au and ligand atoms in $[AuX_2]^-$ (X = H, F–Uus, CN), calculated with different charge density schemes

		Net charge			
	Atom	Hirshfeld[42]	Voronoi[43]	MDC-q[44]	NPA[45]
$[AuF_2]^-$	Au	−0.103	−0.023	−0.038	0.474
	F	−0.448	−0.489	−0.481	−0.737
$[AuCl_2]^-$	Au	−0.090	−0.026	−0.104	0.314
	Cl	−0.455	−0.487	−0.448	−0.657
$[AuBr_2]^-$	Au	−0.090	−0.046	−0.101	0.254
	Br	−0.455	−0.477	−0.449	−0.627
$[AuI_2]^-$	Au	−0.102	−0.102	−0.180	0.169
	I	−0.449	−0.449	−0.410	−0.585
$[AuAt_2]^-$	Au	−0.123	−0.144	−0.211	0.132
	At	−0.438	−0.428	−0.395	−0.566
$[AuUus_2]^-$	Au	−0.157	−0.202	−0.383	0.076
	Uus	−0.422	−0.399	−0.308	−0.538
$[AuH_2]^-$	Au	−0.394	−0.071	−0.372	−0.048
	H	−0.303	−0.464	−0.314	−0.476
$[Au(CN)_2]^-$	Au	0.045	0.107	0.218	0.318
	C	−0.169	−0.200	−0.211	−0.143

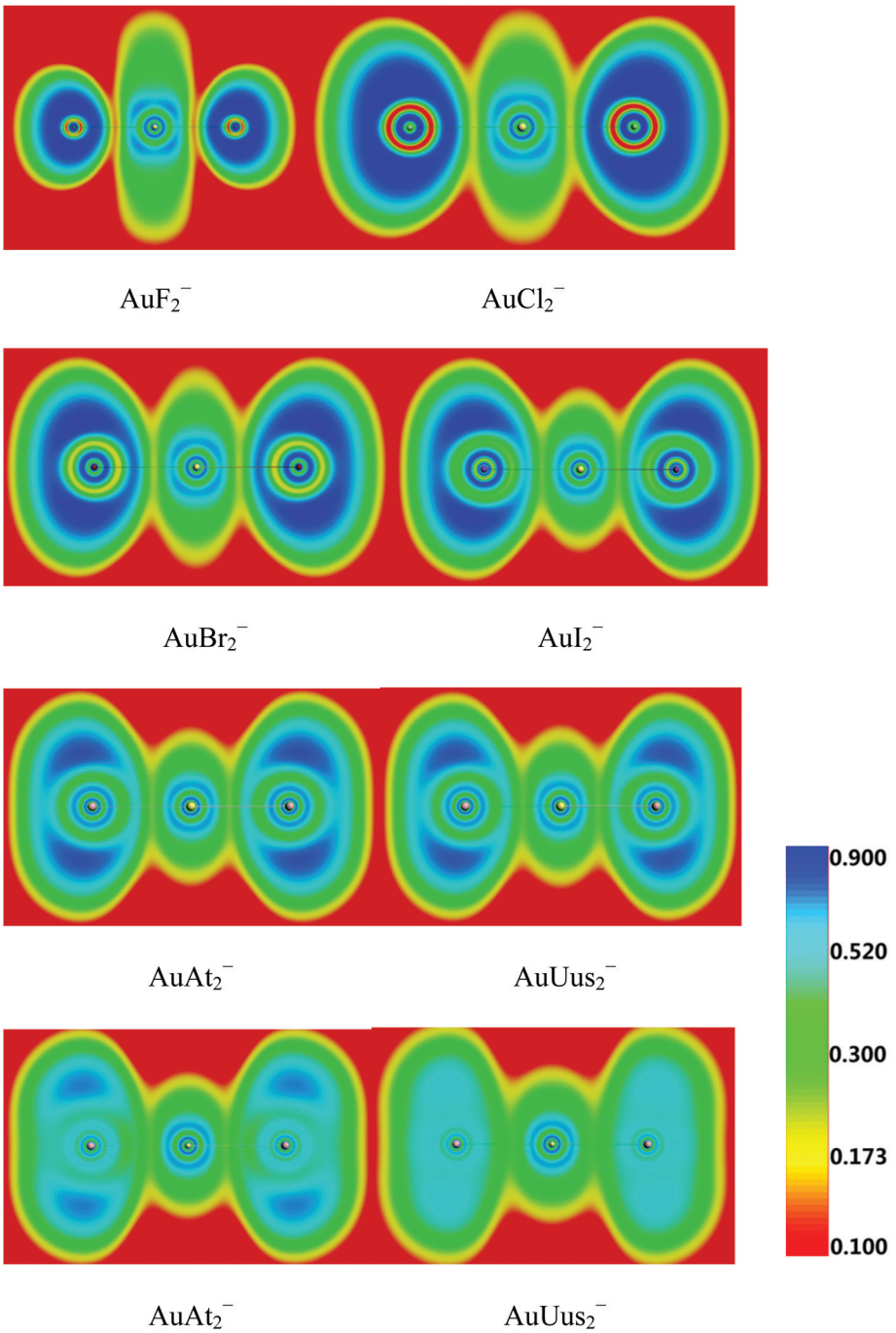

Fig. 1 The electron localization functions (ELFs) of $[AuX_2]^-$ (X = F–Uus). The results of the first three rows are based on the SR-ZORA calculated densities and those of the last row are based on the SO-ZORA densities.

same trends of covalency from X = F to I, but with decreasing covalency from I to At. It should be noted that, compared with PBE calculations, the NBO bonding orbitals at the CCSD level have less contributions from gold, and in consequence leading to respectively lower covalent bond order in the NRT results.

To understand the linear geometry and the covalency trend in the Au(I)–halogen complexes, we present the molecular orbital energy levels and the isocontour surfaces of $[AuX_2]^-$ in Fig. 2 and 3, respectively. In general, the np AOs of the two halogen atoms transform into σ_g, σ_u, π_g and π_u MOs in $[X\cdots X]^{2-}$. The Au 5d orbitals transform as $\sigma_g + \pi_g + \delta_g$ in $D_{\infty h}$ symmetry. Due to the strong relativistic effects in gold, the sd_{z^2} hybridization is enhanced (assuming the linear molecule is oriented along the *z*-axis).[1b] The Au 5d atomic orbitals would not be involved in net bonding with main-group elements if there were no sd hybridizations. Pictorially, the sd hybridiz-

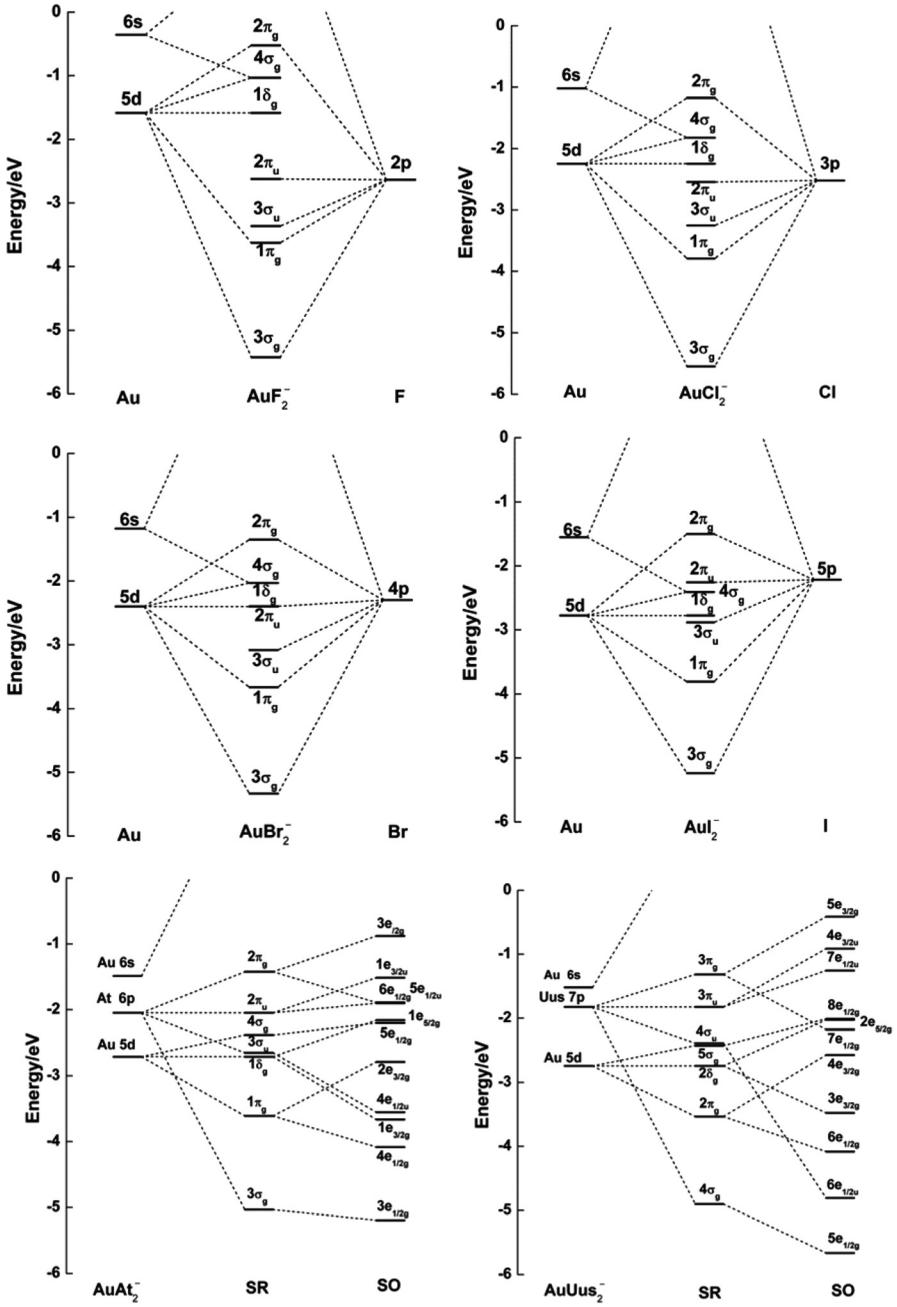

Fig. 2 The energy levels of $[AuX_2]^-$ (X = F–Uus). The calculated Kohn–Sham MO energies are used, with the atomic orbital energies aligned with the non-bonding MO energies. The results for X = F–I are based on the ADF SR-ZORA PBE/TZ2P calculations, while spin–orbit splittings are also included for At and Uus.

ation results in two hybrid orbitals, which are 180° relative to each other. The geometrical characters of the two sd hybrid orbitals lead to the most effective overlaps with the σ_g orbital of $[X\cdots X]^{2-}$ if the $[AuX_2]^-$ complex is linear. The linear structure also maximizes overlaps of orbitals with π symmetry, *i.e.*, between Au $5d_\pi$ AOs and π_g orbitals of $[X\cdots X]^{2-}$, while minimizing the electrostatic repulsion between the two negatively charged ligands. As shown in the energy levels in Fig. 2 and MOs in Fig. 3, the main contributions to bonding interactions come from the lowest σ_g and π_g molecular orbitals. In addition, the σ_u orbital is stabilized through the interaction with Au 6p orbitals, as shown in Fig. 2. The lowest σ_g orbital is derived from the Au sd_{z^2} hybridized orbital and the p_z AOs of the halogen atoms, resulting in a strong σ bond. The lowest π_g orbitals are resulted from the Au $5d_\pi$ AOs with π_g orbitals of $[X\cdots X]^{2-}$ and these orbitals also entail strongly bonding interactions. The 2p orbital of F is relatively contracted and its energy is very low, resulting in the largest orbital energy difference between the Au 6s orbital and the valent np orbitals of the halogens. These factors underlie the more ionic bonding

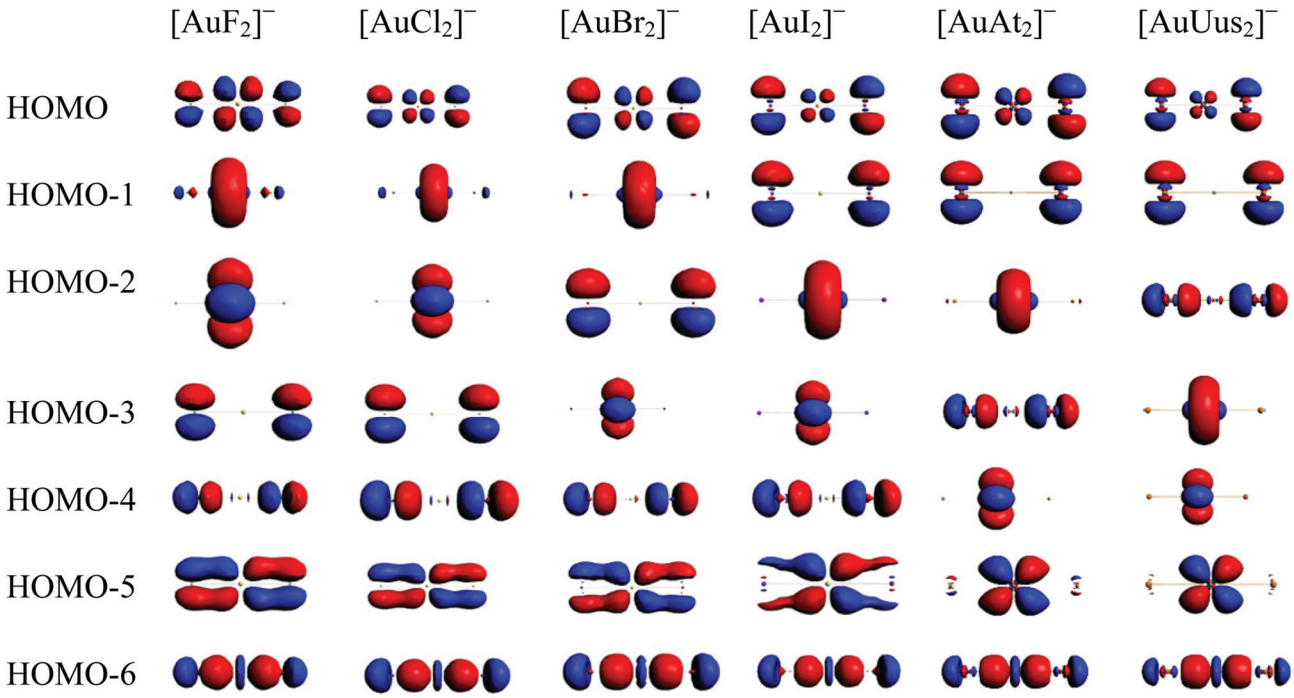

Fig. 3 Molecular orbitals (MOs) of $[AuX_2]^-$ (X = F, Cl, Br, I, At, and Uus) (isosurface = 0.05 a.u.). From the first row to last row, the MOs for AuF_2^- are $2\pi_g$, $4\sigma_g$, $1\delta_g$, $2\pi_u$, $3\sigma_u$, $1\pi_g$ and $3\sigma_g$ respectively.

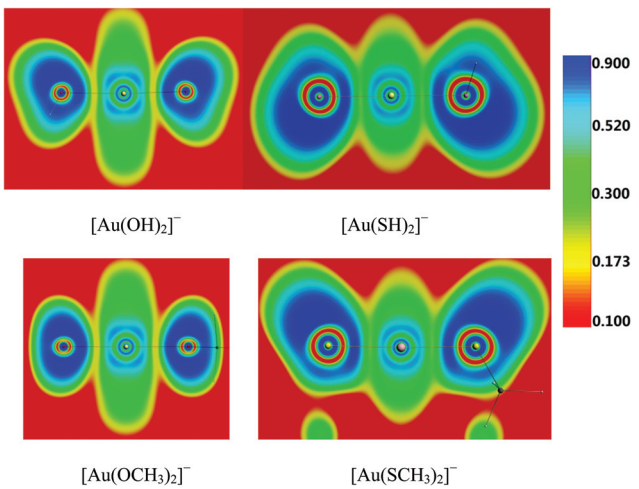

Fig. 4 The electron localization functions (ELFs) of $[AuX_2]^-$ (X = OH, SH, OCH_3 and SCH_3).

between Au and F compared to other halogens, as seen in Table 3 and shown from the calculated atomic charges in Table 6. For heavy halogen atoms, the energies of the I 5p, At 6p, and Uus 7p AOs are almost comparable to that of the 6s orbital of Au, consistent with the increased covalency between Au and halogens from F to Uus.

The valence AOs of the very heavy halogen elements, At and Uus, have substantial spin–orbit effects, which have significant influences on the Au–X bonding. ELF analyses (Fig. 1) and NRT calculations (Table 3) both reveal clear covalent characters in the Au–At and Au–Uus bonding. A comparison of the ELFs between SR-ZORA and SO-ZORA calculation in Fig. 1 shows that the covalent character has been enhanced by the spin–orbit effect, in particular, for the Au–Uus bonds. The molecular orbitals of $[AuAt_2]^-$ and $[AuUus_2]^-$ in Fig. 3 and the energy levels in Fig. 2 show that the most effective bonding orbitals are the same as the light halogen atoms, *i.e.*, the σ_g and π_g orbitals, except that the σ bond is strengthened and the π bond is clearly weakened in comparison with the light halogen ligands. The bonding σ_g orbital in $[AuUus_2]^-$ is significantly stabilized after the incorporation of the spin–orbit effects. One plausible reason is through the mixing between the spin–orbit split orbitals, which stabilizes the net bonding orbitals and enhances the Au–Uus bonding in $[AuUus_2]^-$.

The decomposition of the bonding energy between Au and the ligand provides further insight into the nature of the Au–halogen bonding. Here the interaction between XAu and X^- is investigated by the EDA calculations. In an ideal ionic bond, there would be no orbital interaction energy between XAu and X^-, according to eqn (1), that is, the steric interaction energy reflects the ionic interaction strength between the two fragments. As shown in Table 5, from F to Uus, the steric interaction energy monotonously increases from −1.58 eV to −0.18 eV, showing decreasing ionic contributions to the total bonding. On the other hand, the orbital interaction between XAu and X^- indicates the degree of covalency between Au and X. Table 5 also shows that along the series from F to Uus, the ratio of the orbital interaction energy relative to the total interaction energy increases.

Table 7 Calculated vibrational frequencies and normalized vibrational frequencies (NVF) for $[AuX_2]^-$ at the PBE level

	Vibrational frequencies (cm^{-1})			NVF[a] (cm^{-1})		
	σ_g	σ_u	π_u	σ_g	σ_u	π_u
$[AuF_2]^-$	484	514	176	237	310	105
$[AuCl_2]^-$	310	330	103	206	253	79
$[AuBr_2]^-$	194	238	69	194	238	69
$[AuI_2]^-$	143	194	52	181	218	58
$[AuAt_2]^-$	105	169	43	172	210	54
$[AuUus_2]^-$	85	154	37	162	199	48

[a] The normalized vibrational frequencies were calculated by assuming that all X have the same mass as Br.[13c]

All bonding and orbital analyses show that the covalency of Au(I)–X bond increases from the F to Uus, giving rise to the strongest covalent bond in the linear $[AuUus_2]^-$ complex. However, EDA calculations show that the total bonding energy decreases from F to Uus in the $[AuX_2]^-$ complexes because of the reduced stabilization arising from the ionic electrostatic interactions. The calculated vibrational frequencies and normalized vibrational frequencies listed in Table 7 reveal the same trend. The frequencies of the symmetric stretching mode and the bending mode decrease. Table 2 shows that the most notable increase in the Au–X bond length occurs from F to Cl, by 0.317 Å at the CCSD(T)/AVTZ level, whereas the Au–X bond length change is only 0.114 Å from Cl to Br. A similar phenomenon is also observed in other bonding properties shown in Tables 3–5, where the sharpest change also occurs from F to Cl. The special behavior of $[AuF_2]^-$ should be due to the compact fluorine atom as compared with the large chlorine atom,[39] while the atomic radius changes down the periodic table after Cl is relatively smooth. The short Au–F bond length and large electronegativity of F lead to apparent ionic characters in the Au–F bond and strong attraction between the positively charged Au in the AuF fragment and F^-, resulting in the strengthened bond as Table 5 shows.

$[AuX_2]^-$: X = non-halogen ligands

The $[AuX_2]^-$ complexes with non-halogen ligands are also linear or quasi-linear, both at the levels of density functional theory and wave function theory, as presented in Tables 1 and 2. Similar to the halogen complexes, MP2 generally predicts short Au–X bond lengths, while CCSD produces relatively long Au–X bond lengths. The linearity of these complexes are the same as the halogen atoms and all Au–X bondings have noticeable contributions from the Au sd hybridized AOs, as indicated in the NBO analyses listed in Tables 3 and 4. The chalcogen group ligands have the same trends as in the halogen group. Both the ELFs (Fig. 4) and NRT analyses (Tables 3 and 4) show that the Au–S bond has more covalent characters than the Au–O bond, as indicated by the comparison of OH with SH and OCH_3 with SCH_3. NBO and NRT calculations (Tables 3 and 4) suggest that the Au–S bond has the most apparent covalent character among the ligands we studied in this paper. Table 4 shows that the covalent bond order for the Au–S bond in $[Au(SH)_2]^-$ is 0.272 at the level of CCSD-DKH2, which implies significant

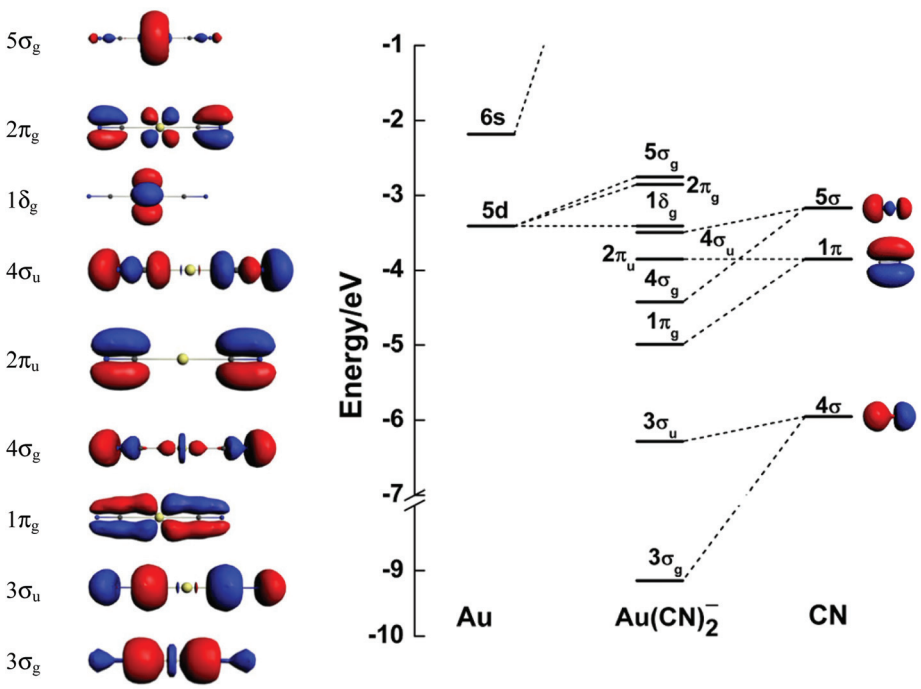

Fig. 5 Molecular orbitals and energy levels of $[Au(CN)_2]^-$ with $5\sigma_g$ as the HOMO (isosurface = 0.05 a.u.).

covalent character in the Au–S bond. Thiolate ligands are widely used to protect gold nanoparticles and the stability of the Au–S bond is ascribed to the covalent bonding nature.[13d]

The bonding situations in $[AuH_2]^-$ and $[Au(CN)_2]^-$ are also investigated here for comparison. Our calculated bond length of Au–CN in $[Au(CN)_2]^-$ is comparable with previous work at both the MP2 and CCSD(T) level.[40] The photoelectron spectra and bonding analyses for these two complexes have been reported recently.[13b,e] $[Au(CN)_2]^-$ is the most stable known Au(I) complex and it has been used in gold extraction since ancient times. It has also been used as an ideal unit to explore the principles of using aurophilicity for the supermolecular design.[12b] The stability of $[Au(CN)_2]^-$ has been attributed to strong covalent interactions[13b] and large relativistic effects.[2c] Strong covalent bonding has also been found in the $[AuH_2]^-$ complex, in addition to an unprecedented H 2p orbital contribution to the Au–H bonding.[12e] The calculated atomic charges for these two complexes are also presented in Table 6. The linear geometry of $[Au(CN)_2]^-$ can also be attributed to maximal overlaps in both the σ-symmetry and π-symmetry orbitals between Au(I) and $[CN\cdots CN]^{2-}$, similar to the cases of halogen complexes. The MOs and energy level diagram of $[Au(CN)_2]^-$ are shown in Fig. 5.

The EDA results in Table 5 give important insight into the special stability of the Au–CN and Au–S bonds. Compared to the halogen ligands, these ligands have very large orbital interaction energies with Au(I). Sulfur-containing ligands have remarkable covalent interactions with Au(I) among the selected ligands studied in this article. The relationship between the stability of the Au–S bond and covalency has been discussed previously.[13d] For the special case of CN, all theoretical methods in Table 6 give a positively charged Au and negatively charged C. As shown in the EDA results (Table 5), apart from the very large orbital interaction energy it also has a large steric interaction with Au(I), these two effects give Au–CN exceptional bonding interactions and unusual stability, consistent with the conclusions reported by Frenking and coworkers who carried out an extensive analysis of the structure and bonding of group 11 cyanide and isocyanide.[41]

Conclusions

Through relativistic quantum chemical calculations and theoretical analyses, we have systematically studied the chemical bonding between Au(I) and a variety of ligands in linear $[AuX_2]^-$ complexes. We find that the most prominent bonding contribution occurs between the Au sd hybrid orbitals and the relevant ligand orbitals, resulting in a strong σ bond. The Au–X π interaction also stabilizes the molecules. The linear X–Au–X geometry maximizes both the σ and π overlaps in the bonding orbitals between Au(I) and X, while minimizing the repulsion of the two negatively charged ligands. Periodic trends are found in the bond length and covalent nature of the Au–X bond for X = F to Uus. Despite the increase of covalency in the Au–X bonds, the overall bonding energies and vibrational frequencies of the stretching and bending modes decrease from F to Uus due to the reduced electrostatic interactions in $[AuX_2]^-$ complexes. We show that the spin–orbit effects enhance the covalency in the Au–Uus bond. The special stability in the well-known $[Au(CN)_2]^-$ complex is found to arise from the combined effects of both large covalent and ionic interactions between Au(I) and the two CN^- ligands.

Acknowledgements

The theoretical work was supported by NKBRSF (2011CB932400) and NSFC (11079006, 21221062, 21101098, 21433005) of China. The calculations were performed at the Tsinghua National Laboratory for Information Science and Technology, and Shanghai Supercomputing Center. L.S.W. wishes to thank the US National Science Foundation (CHE-1263745) for support of this work.

References

1 (*a*) P. Pyykkö and J. P. Desclaux, Relativity and the periodic system of elements, *Acc. Chem. Res.*, 1979, **12**(8), 276–281; (*b*) P. Pyykkö, Relativistic effects in structural chemistry, *Chem. Rev.*, 1988, **88**(3), 563–594; (*c*) P. Pyykkö, Relativistic Effects in Chemistry: More Common Than You Thought, *Annu. Rev. Phys. Chem.*, 2012, **63**(1), 45–64; (*d*) J. Autschbach, S. Siekierski, M. Seth, P. Schwerdtfeger and W. H. E. Schwarz, Dependence of relativistic effects on electronic configuration in the neutral atoms of d- and f-block elements, *J. Comput. Chem.*, 2002, **23**(8), 804–813.

2 (*a*) P. Schwerdtfeger, M. Dolg, W. H. E. Schwarz, G. A. Bowmaker and P. D. W. Boyd, Relativistic effects in gold chemistry. I. Diatomic gold compounds, *J. Chem. Phys.*, 1989, **91**(3), 1762–1774; (*b*) P. Schwerdtfeger, Relativistic effects in gold chemistry. 2. The stability of complex halides of gold(III), *J. Am. Chem. Soc.*, 1989, **111**(18), 7261–7262; (*c*) P. Schwerdtfeger, P. D. W. Boyd, A. K. Burrell, W. T. Robinson and M. J. Taylor, Relativistic effects in gold chemistry. 3. Gold(I) complexes, *Inorg. Chem.*, 1990, **29**(18), 3593–3607; (*d*) P. Schwerdtfeger, P. D. W. Boyd, S. Brienne and A. K. Burrell, Relativistic effects in gold chemistry. 4. Gold(III) and gold(V) compounds, *Inorg. Chem.*, 1992, **31**(16), 3411–3422; (*e*) P. Schwerdtfeger and G. A. Bowmaker, Relativistic effects in gold chemistry. V. Group 11 dipole polarizabilities and weak bonding in monocarbonyl compounds, *J. Chem. Phys.*, 1994, **100**(6), 4487–4497; (*f*) R. Wesendrup, J. K. Laerdahl and P. Schwerdtfeger, Relativistic effects in gold chemistry. VI. Coupled cluster calculations for the isoelectronic series $AuPt^-$, Au^2, and $AuHg^+$, *J. Chem. Phys.*, 1999, **110**(19), 9457–9462; (*g*) P. Schwerdtfeger, Relativistic effects in properties of gold, *Heteroat. Chem.*, 2002, **13**(6), 578–584.

3 P. Schwerdtfeger, Relativistic and electron-correlation contributions in atomic and molecular properties: benchmark

calculations on Au and Au_2, *Chem. Phys. Lett.*, 1991, **183**(5), 457–463.

4 E. M. Fernández, J. M. Soler, I. L. Garzón and L. C. Balbás, Trends in the structure and bonding of noble metal clusters, *Phys. Rev. B: Condens. Matter*, 2004, **70**(16), 165403.

5 (*a*) F. A. Cotton, G. Wilkinson, C. A. Murillo and M. Bochmann, *Advanced Inorganic Chemistry*, John Wiley & Sons, 6th edn, 1999; (*b*) M. Seth, P. Schwerdtfeger and K. Fægri, The chemistry of superheavy elements. III. Theoretical studies on element 113 compounds, *J. Chem. Phys.*, 1999, **111**(14), 6422–6433.

6 (*a*) M. Haruta, T. Kobayashi, H. Sano and N. Yamada, Novel Gold Catalysts for the Oxidation of Carbon Monoxide at a Temperature far Below 0 °C, *Chem. Lett.*, 1987, **16**(2), 405–408; (*b*) M. Valden, X. Lai and D. W. Goodman, Onset of Catalytic Activity of Gold Clusters on Titania with the Appearance of Nonmetallic Properties, *Science*, 1998, **281**(5383), 1647–1650; (*c*) D. J. Gorin and F. D. Toste, Relativistic effects in homogeneous gold catalysis, *Nature*, 2007, **446**(7134), 395–403.

7 C. F. Shaw, Gold-Based Therapeutic Agents, *Chem. Rev.*, 1999, **99**(9), 2589–2600.

8 L. Belpassi, I. Infante, F. Tarantelli and L. Visscher, The Chemical Bond between Au(I) and the Noble Gases. Comparative Study of NgAuF and $NgAu^+$ (Ng = Ar, Kr, Xe) by Density Functional and Coupled Cluster Methods, *J. Am. Chem. Soc.*, 2007, **130**(3), 1048–1060.

9 (*a*) P. Pyykkö, Theoretical Chemistry of Gold, *Angew. Chem., Int. Ed.*, 2004, **43**(34), 4412–4456; (*b*) P. Pyykkö, Theoretical chemistry of gold. II, *Inorg. Chim. Acta*, 2005, **358**(14), 4113–4130; (*c*) P. Pyykkö, Theoretical chemistry of gold. III, *Chem. Soc. Rev.*, 2008, **37**(9), 1967–1997.

10 J. J. Vittal and R. J. Puddephatt, Gold: Inorganic & Coordination Chemistry, In *Encyclopedia of Inorganic and Bioinorganic Chemistry*, John Wiley & Sons Ltd, 2011.

11 J. H. Teles, S. Brode and M. Chabanas, Cationic Gold(I) Complexes: Highly Efficient Catalysts for the Addition of Alcohols to Alkynes, *Angew. Chem., Int. Ed.*, 1998, **37**(10), 1415–1418.

12 (*a*) P. Pyykkö, Strong Closed-Shell Interactions in Inorganic Chemistry, *Chem. Rev.*, 1997, **97**(3), 597–636; (*b*) M. A. Rawashdeh-Omary, M. A. Omary and H. H. Patterson, Oligomerization of $Au(CN)_2^-$ and $Ag(CN)_2^-$ Ions in Solution via Ground-State Aurophilic and Argentophilic Bonding, *J. Am. Chem. Soc.*, 2000, **122**(42), 10371–10380; (*c*) W. J. Hunks, M. C. Jennings and R. J. Puddephatt, Supramolecular gold(I) thiobarbiturate chemistry: Combining aurophilicity and hydrogen bonding to make polymers, sheets, and networks, *Inorg. Chem.*, 2002, **41**(17), 4590–4598; (*d*) P. Pyykkö, X. G. Xiong and J. Li, Aurophilic attractions between a closed-shell molecule and a gold cluster, *Faraday Discuss.*, 2011, **152**, 169–178; (*e*) H. Schmidbaur and A. Schier, Aurophilic interactions as a subject of current research: an up-date, *Chem. Soc. Rev.*, 2012, **41**(1), 370–412.

13 (*a*) H.-J. Zhai, C. Bürgel, V. Bonacic-Koutecky and L. S. Wang, Probing the Electronic Structure and Chemical Bonding of Gold Oxides and Sulfides in AuO_n^- and AuS_n^- (n = 1, 2), *J. Am. Chem. Soc.*, 2008, **130**(28), 9156–9167; (*b*) X.-B. Wang, Y.-L. Wang, J. Yang, X.-P. Xing, J. Li and L. S. Wang, Evidence of Significant Covalent Bonding in $Au(CN)_2^-$, *J. Am. Chem. Soc.*, 2009, **131**(45), 16368–16370; (*c*) Y.-L. Wang, X.-B. Wang, X.-P. Xing, F. Wei, J. Li and L. S. Wang, Photoelectron Imaging and Spectroscopy of MI_2^- (M = Cs, Cu, Au): Evolution from Ionic to Covalent Bonding, *J. Phys. Chem. A*, 2010, **114**(42), 11244–11251; (*d*) C.-G. Ning, X.-G. Xiong, Y.-L. Wang, J. Li and L. S. Wang, Probing the electronic structure and chemical bonding of the "staple" motifs of thiolate gold nanoparticles: $Au(SCH_3)_2^-$ and $Au_2(SCH_3)_3^-$, *Phys. Chem. Chem. Phys.*, 2012, **14**(26), 9323–9329; (*e*) H.-T. Liu, Y.-L. Wang, X.-G. Xiong, P. D. Dau, Z. A. Piazza, D.-L. Huang, C.-Q. Xu, J. Li and L. S. Wang, The electronic structure and chemical bonding in gold dihydride: AuH_2^- and AuH_2, *Chem. Sci.*, 2012, **3**(11), 3286–3295; (*f*) H.-T. Liu, X.-G. Xiong, P. D. Dau, Y.-L. Wang, J. Li and L. S. Wang, The mixed cyanide halide Au(I) complexes: $[XAuCN]^-$ (X = F, Cl, Br, and I): evolution from ionic to covalent bonding, *Chem. Sci.*, 2011, **2**(11), 2101–2108.

14 T. Hangele, M. Dolg, M. Hanrath, X. Cao and P. Schwerdtfeger, Accurate relativistic energy-consistent pseudopotentials for the superheavy elements 111 to 118 including quantum electrodynamic effects, *J. Chem. Phys.*, 2012, **136**(21), 214105.

15 L. S. Wang, Covalent gold, *Phys. Chem. Chem. Phys.*, 2010, **12**(31), 8694–8705.

16 A. D. Becke and K. E. Edgecombe, A simple measure of electron localization in atomic and molecular systems, *J. Chem. Phys.*, 1990, **92**(9), 5397–5403.

17 (*a*) E. D. Glendening and F. Weinhold, Natural resonance theory: I. General formalism, *J. Comput. Chem.*, 1998, **19**(6), 593–609; (*b*) E. D. Glendening and F. Weinhold, Natural resonance theory: II. Natural bond order and valency, *J. Comput. Chem.*, 1998, **19**(6), 610–627.

18 M. v. Hopffgarten and G. Frenking, Energy decomposition analysis, *Wiley Interdiscip. Rev.: Comput. Mol. Sci.*, 2012, **2**(1), 43–62.

19 J. P. Perdew, K. Burke and M. Ernzerhof, Generalized Gradient Approximation Made Simple, *Phys. Rev. Lett.*, 1996, **77**(18), 3865–3868.

20 (*a*) G. te Velde, F. M. Bickelhaupt, E. J. Baerends, C. Fonseca Guerra, S. J. A. van Gisbergen, J. G. Snijders and T. Ziegler, Chemistry with ADF, *J. Comput. Chem.*, 2001, **22**(9), 931–967; (*b*) C. Fonseca Guerra, J. G. Snijders, G. te Velde and E. J. Baerends, Towards an order-N DFT method, *Theor. Chem. Acc.*, 1998, **99**(6), 391–403.

21 (*a*) E. v. Lenthe, E. J. Baerends and J. G. Snijders, Relativistic regular two-component Hamiltonians, *J. Chem. Phys.*, 1993, **99**(6), 4597–4610; (*b*) E. v. Lenthe, E. J. Baerends and J. G. Snijders, Relativistic total energy using regular approximations, *J. Chem. Phys.*, 1994, **101**(11), 9783–9792;

(*c*) E. v. Lenthe, A. Ehlers and E.-J. Baerends, Geometry optimizations in the zero order regular approximation for relativistic effects, *J. Chem. Phys.*, 1999, **110**(18), 8943–8953.

22 E. v. Lenthe, J. G. Snijders and E. J. Baerends, The zero-order regular approximation for relativistic effects: The effect of spin–orbit coupling in closed shell molecules, *J. Chem. Phys.*, 1996, **105**(15), 6505–6516.

23 C. Møller and M. S. Plesset, Note on an Approximation Treatment for Many-Electron Systems, *Phys. Rev.*, 1934, **46**(7), 618–622.

24 S. Grimme, Improved second-order Møller–Plesset perturbation theory by separate scaling of parallel- and antiparallel-spin pair correlation energies, *J. Chem. Phys.*, 2003, **118**(20), 9095–9102.

25 C. Hampel, K. A. Peterson and H.-J. Werner, A comparison of the efficiency and accuracy of the quadratic configuration interaction (QCISD), coupled cluster (CCSD), and Brueckner coupled cluster (BCCD) methods, *Chem. Phys. Lett.*, 1992, **190**(1–2), 1–12.

26 J. D. Watts, J. Gauss and R. J. Bartlett, Coupled-cluster methods with noniterative triple excitations for restricted open-shell Hartree-Fock and other general single determinant reference functions. Energies and analytical gradients, *J. Chem. Phys.*, 1993, **98**(11), 8718–8733.

27 H.-J. Werner, *MOLPRO, 2012.1*, a package of *ab initio* programs; see: http://www.molpro.net.

28 (*a*) D. Figgen, G. Rauhut, M. Dolg and H. Stoll, Energy-consistent pseudopotentials for group 11 and 12 atoms: adjustment to multi-configuration Dirac–Hartree–Fock data, *Chem. Phys.*, 2005, **311**(1–2), 227–244; (*b*) K. A. Peterson and C. Puzzarini, Systematically convergent basis sets for transition metals. II. Pseudopotential-based correlation consistent basis sets for the group 11 (Cu, Ag, Au) and 12 (Zn, Cd, Hg) elements, *Theor. Chem. Acc.*, 2005, **114**(4–5), 283–296.

29 K. A. Peterson, D. Figgen, E. Goll, H. Stoll and M. Dolg, Systematically convergent basis sets with relativistic pseudopotentials. II. Small-core pseudopotentials and correlation consistent basis sets for the post-d group 16–18 elements, *J. Chem. Phys.*, 2003, **119**(21), 11113–11123.

30 K. A. Peterson, B. C. Shepler, D. Figgen and H. Stoll, On the Spectroscopic and Thermochemical Properties of ClO, BrO, IO, and Their Anions, *J. Phys. Chem. A*, 2006, **110**(51), 13877–13883.

31 (*a*) J. Thom and H. Dunning, Gaussian basis sets for use in correlated molecular calculations. I. The atoms boron through neon and hydrogen, *J. Chem. Phys.*, 1989, **90**(2), 1007–1023; (*b*) D. E. Woon, J. Thom and H. Dunning, Gaussian basis sets for use in correlated molecular calculations. III. The atoms aluminum through argon, *J. Chem. Phys.*, 1993, **98**(2), 1358–1371; (*c*) A. K. Wilson, D. E. Woon, K. A. Peterson, J. Thom and H. Dunning, Gaussian basis sets for use in correlated molecular calculations. IX. The atoms gallium through krypton, *J. Chem. Phys.*, 1999, **110**(16), 7667–7676.

32 E. D. Glendening, J. K. Badenhoop, A. E. Reed, J. E. Carpenter, J. A. Bohmann, C. M. Morales and F. Weinhold, *NBO 5.0*, Theoretical Chemistry Institute, University of Wisconsin, Madison, W., 2001, http://www.chem.wisc.edu/~nbo5.

33 M. J. Frisch, G. W. Trucks, H. B. Schlegel, G. E. Scuseria, M. A. Robb, J. R. Cheeseman, G. Scalmani, V. Barone, B. Mennucci, G. A. Petersson, H. Nakatsuji, M. Caricato, X. Li, H. P. Hratchian, A. F. Izmaylov, J. Bloino, G. Zheng, J. L. Sonnenberg, M. Hada, M. Ehara, K. Toyota, R. Fukuda, J. Hasegawa, M. Ishida, T. Nakajima, Y. Honda, O. Kitao, H. Nakai, T. Vreven, J. A. Montgomery, Jr., J. E. Peralta, F. Ogliaro, M. Bearpark, J. J. Heyd, E. Brothers, K. N. Kudin, V. N. Staroverov, R. Kobayashi, J. Normand, K. Raghavachari, A. Rendell, J. C. Burant, S. S. Iyengar, J. Tomasi, M. Cossi, N. Rega, J. M. Millam, M. Klene, J. E. Knox, J. B. Cross, V. Bakken, C. Adamo, J. Jaramillo, R. Gomperts, R. E. Stratmann, O. Yazyev, A. J. Austin, R. Cammi, C. Pomelli, J. W. Ochterski, R. L. Martin, K. Morokuma, V. G. Zakrzewski, G. A. Voth, P. Salvador, J. J. Dannenberg, S. Dapprich, A. D. Daniels, O. Farkas, J. B. Foresman, J. V. Ortiz, J. Cioslowski and D. J. Fox, *Gaussian 09, Revision A.02*, Gaussian Inc., Wallingford CT, 2009.

34 A. I. Krylov, C. D. Sherrill and M. Head-Gordon, Excited states theory for optimized orbitals and valence optimized orbitals coupled-cluster doubles models, *J. Chem. Phys.*, 2000, **113**(16), 6509–6527.

35 F. Neese, The ORCA program system, *Wiley Interdiscip. Rev.: Comput. Mol. Sci.*, 2012, **2**(1), 73–78.

36 (*a*) D. A. Pantazis, X.-Y. Chen, C. R. Landis and F. Neese, All-Electron Scalar Relativistic Basis Sets for Third-Row Transition Metal Atoms, *J. Chem. Theor. Comput.*, 2008, **4**(6), 908–919; (*b*) D. Pantazis and F. Neese, All-electron scalar relativistic basis sets for the 6p elements, *Theor. Chem. Acc.*, 2012, **131**(11), 1–7.

37 S. Mishra, Theoretical Calculation of the Photodetachment Spectra of $XAuY^-$ (X, Y = Cl, Br, and I), *J. Phys. Chem. A*, 2007, **111**(37), 9164–9168.

38 M. Seth, F. Cooke, P. Schwerdtfeger, J.-L. Heully and M. Pelissier, The chemistry of the superheavy elements. II. The stability of high oxidation states in group 11 elements: Relativistic coupled cluster calculations for the di-, tetra- and hexafluoro metallates of Cu, Ag, Au, and element 111, *J. Chem. Phys.*, 1998, **109**(10), 3935–3943.

39 P. Pyykkö and M. Atsumi, Molecular Double-Bond Covalent Radii for Elements Li–E112, *Chem. – Eur. J.*, 2009, **15**(46), 12770–12779.

40 P. Schwerdtfeger and M. Lein, Theoretical Chemistry of Gold – From Atoms to Molecules, Clusters, Surfaces and the Solid State, In *Gold Chemistry*, Wiley-VCH Verlag GmbH & Co. KGaA, 2009, pp. 183–247.

41 O. Dietz, V. M. Rayón and G. Frenking, Molecular Structures, Bond Energies, and Bonding Analysis of Group 11 Cyanides TM(CN) and Isocyanides TM(NC) (TM = Cu, Ag, Au), *Inorg. Chem.*, 2003, **42**(16), 4977–4984.

42 F. L. Hirshfeld, Bonded-atom fragments for describing molecular charge densities, *Theor. Chim. Acta*, 1977, **44**(2), 129–138.
43 F. M. Bickelhaupt, N. J. R. van Eikema Hommes, C. Fonseca Guerra and E. J. Baerends, The Carbon −Lithium Electron Pair Bond in $(CH_3Li)_n$ (n = 1, 2, 4), *Organometallics*, 1996, **15**(13), 2923–2931.
44 M. Swart, P. T. van Duijnen and J. G. Snijders, A charge analysis derived from an atomic multipole expansion, *J. Comput. Chem.*, 2001, **22**(1), 79–88.
45 A. E. Reed, R. B. Weinstock and F. Weinhold, Natural population analysis, *J. Chem. Phys.*, 1985, **83**(2), 735–746.